A&A 639, A25 (2020)
https://doi.org/10.1051/0004-6361/202037794

Astronomy & Astrophysics

Multiconfiguration Dirac-Hartree-Fock calculations of Landé *g*-factors for ions of astrophysical interest: B II, C I–IV, Al I–II, Si I–IV, P II, S II, Cl III, Ar IV, Ca I, Ti II, Zr III, and Sn II*

W. Li[1], P. Rynkun[2], L. Radžiūtė[2], G. Gaigalas[2], B. Atalay[3,4], A. Papoulia[1,3], K. Wang[5], H. Hartman[1], J. Ekman[1], T. Brage[3], C. Y. Chen[6], and P. Jönsson[1]

[1] Department of Materials Science and Applied Mathematics, Malmö University, 20506 Malmö, Sweden
e-mail: wenxian.li@mau.se
[2] Institute of Theoretical Physics and Astronomy, Vilnius University, Saulėtekio Av. 3, 10222 Vilnius, Lithuania
[3] Division of Mathematical Physics, Lund University, Post Office Box 118, 22100 Lund, Sweden
[4] Department of Physics, Çanakkale Onsekiz Mart University, Çanakkale, Turkey
[5] Hebei Key Lab of Optic-electronic Information and Materials, The College of Physics Science and Technology, Hebei University, Baoding 071002, PR China
[6] Shanghai EBIT Lab, Key Laboratory of Nuclear Physics and Ion-beam Application, Institute of Modern Physics, Department of Nuclear Science and Technology, Fudan University, Shanghai 200433, PR China

Received 21 February 2020 / Accepted 4 May 2020

ABSTRACT

Aims. The Landé g-factor is an important parameter in astrophysical spectropolarimetry, used to characterize the response of a line to a given value of the magnetic field. The purpose of this paper is to present accurate Landé g-factors for states in B II, C I–IV, Al I–II, Si I–IV, P II, S II, Cl III, Ar IV, Ca I, Ti II, Zr III, and Sn II.

Methods. The multiconfiguration Dirac-Hartree-Fock and relativistic configuration interaction methods, which are implemented in the general-purpose relativistic atomic structure package GRASP2K, are employed in the present work to compute the Landé g-factors for states in B II, C I–IV, Al I–II, Si I–IV, P II, S II, Cl III, Ar IV, Ca I, Ti II, Zr III, and Sn II. The accuracy of the wave functions for the states, and thus the accuracy of the resulting Landé g-factors, is evaluated by comparing the computed excitation energies and energy separations with the National Institute of Standards and Technology (NIST) recommended data.

Results. All excitation energies are in very good agreement with the NIST values except for Ti II, which has an average difference of 1.06%. The average uncertainty of the energy separations is well below 1% except for the even states of Al I; odd states of Si I, Ca I, Ti II, Zr III; and even states of Sn II for which the relative differences range between 1% and 2%. Comparisons of the computed Landé g-factors are made with available NIST data and experimental values. Analysing the LS-composition of the wave functions, we quantify the departures from LS-coupling and summarize the states for which there is a difference of more than 10% between the computed Landé g-factor and the Landé g-factor in pure LS-coupling. Finally, we compare the computed Landé g-factors with values from the Kurucz database.

Key words. atomic data – magnetic fields

1. Introduction

Magnetic fields play a fundamental role in astrophysical systems, and thus in the evolution of the Universe. Measurement of the polarization of light as a function of wavelength, known as spectropolarimetry, is the most powerful tool for the accurate determination of magnetic fields in astrophysics. Highly accurate atomic data (e.g. excitation energies, transition rates, oscillator strengths, and Landé g-factors) are essential for interpreting and modelling the spectropolarimetric observations (Judge 2017). The need for atomic data have increased tremendously over the last 20 years with the development of new instrumentation like the *Daniel K. Inouye* Solar Telescope (DKIST, formerly ATST; Keil et al. 2009). The next generation ground-based solar telescopes will also offer spectropolarimetric capabilities covering a broad wavelength range from the visible into the near-infrared, the latter of which is largely unexplored spectroscopically.

When an atom or ion is placed in a magnetic field, level splitting occurs that breaks the degeneracy of the energy levels for the different magnetic quantum numbers. This splitting, known as the Zeeman effect, is caused by the interaction between the magnetic moment of the atom and an external magnetic field (Cowan 1981) and is expressed in terms of the Landé g-factor. Accordingly, the effective Landé g-factor of a spectral line, which can be expressed in terms of the Landé g-factors of the lower and upper levels, is an important parameter in astrophysical spectropolarimetry used to characterize the response of the line to a given value of the magnetic field (Landi Degl'Innocenti 1982; Landi Degl'Innocenti & Landolfi 2004). The effective Landé g-factor, $\overline{g}$, and the second order effective Landé g-factor, $\overline{G}$, are respectively related to the circular and the linear polarization of a spectral line produced by

* Tables 5–23 are only available at the CDS via anonymous ftp to cdsarc.u-strasbg.fr (130.79.128.5) or via http://cdsarc.u-strasbg.fr/viz-bin/cat/J/A+A/639/A25

the Zeeman effect (Landi Degl'Innocenti & Landolfi 2004). For this reason, detailed investigations of the magnetic fields require knowledge of accurate Landé g-factors.

There are a number of measurements of Landé g-factors. In the first half of 20th century massive efforts were made by atomic physicists to establish the energy level structures of atoms and ions from the observed spectral lines. The experimental Landé g-factors were derived from the analysis of Zeeman patterns in individual spectral lines produced in the magnetic fields. These g-factors were collected and made available in the critical compilation by Moore (1949). However, there was a surprising scarcity of reliable data on observed Zeeman patterns among the spectra of the light elements. For example, among the elements studied in this work, the observed g-factors compiled in Moore (1949) are available only for a few states in Ca I and Ti II, which reveals a glaring need of further observations. Later on, Lott et al. (1966) studied the Zeeman effect using strong pulsed magnetic fields and derived the g-factors for a number of states in B I, C I, C III, O II, O III, Mg I, Mg II, Si I, Si III, Si IV, Ca II, and Cu II. Li (1972) measured the Zeeman effect of P II using the electrodeless discharge tubes operated in a field of 32 215 G. The Landé g-factor of the Sn II $5s5p^2\ {}^4P_{1/2}$ level was measured by David et al. (1980) by direct magnetic resonance. As of today there are, to the knowledge of the authors, no experimental efforts to cover the needs of Landé g-factors, and thus they have to be calculated.

If there are no experimental or calculated data available, the Landé g-factors in pure LS-coupling are sometimes used (see Sect. 2). While in many cases this is a good approximation, there are many cases where this fails, thus giving erroneous polarization profiles. One example is the Fe I transition $3d^74p\ {}^5F^o_1$ – $3d^75s\ {}^5F^e_1$ at 7389.398 Å, where the circular polarization is produced by the Zeeman effect due to the non-zero experimental Landé g-factor value, which is instead missing under the LS-coupling scheme because of the zero Landé g-factor (Li et al. 2017). More accurate values of the Landé g-factors are obtained in the intermediate coupling approximation, as described in Sect. 2 below. Using the Cowan code in the intermediate coupling approximation, Biémont et al. (2010) calculated Landé g-factors for elements along the sixth row of the periodic table. These data were collected in the DESIRE database[1]. In this context we should also mention the MCHF/MCDHF database of Froese Fischer for which the Landé g-factors are provided for a few collections[2]. Fully relativistic calculations of Landé g-factors were pioneered by Cheng & Childs (1985) for states of the $4f^N6s^2$ configurations in rare-earth elements. More recently relativistic g-factor calculations have been performed for states in Ne I and Ne II (Fischer et al. 2004) and Si IX (Brage et al. 2000). A full set of g-factors was also calculated for the $n = 2$ states in beryllium-, boron-, carbon-, and nitrogen-like ions (Verdebout et al. 2014).

The purpose of the present work is to compute accurate Landé g-factors for states in B II, C I–IV, Al I–II, Si I–IV, P II, S II, Cl III, Ar IV, Ca I, Ti II, Zr III, and Sn II within the fully relativistic scheme. Looking at the ions and states studied in this work, the National Institute of Standards and Technology (NIST) database (Kramida et al. 2019) reports Landé g-factors for only 3 out of 100 states for C I, 76 out of 106 for P II, 15 out of 99 for Ti II, and 1 out of 22 for Sn II (see Table 1 for a summary).

[1] http://hosting.umons.ac.be/html/agif/databases/desire.html
[2] https://nlte.nist.gov/MCHF/

2. Theory

We start the theory section with a brief discussion of the Breit–Pauli and intermediate coupling approximations, which provide the necessary background for understanding the validity and limitations of the often used pure LS-coupling approximation of the Landé g-factors. The Breit–Pauli and intermediate coupling approximations also provide the theoretical background for the labelling and description of states by the LS-composition, for example as done in the NIST Atomic Spectra Database (Kramida et al. 2019). After this brief discussion we present the fully relativistic theory and show how it links to the Breit–Pauli and intermediate coupling approximations.

2.1. Multiconfiguration wave functions

In the non-relativistic multiconfiguration Hartree–Fock (MCHF) approach the wave function Ψ for a state labelled γLS, where L and S are the total orbital and spin angular quantum numbers and γ represents the configuration and other quantum numbers needed to specify the state, is expanded in terms of configuration state functions (CSFs) with the same LS term:

$$\Psi(\gamma LS) = \sum_j c_j \Phi(\gamma_j LS). \tag{1}$$

The CSFs are constructed from products of one-electron spin orbitals. The radial orbitals and the expansion coefficients of the CSFs are determined by iteratively solving a set of coupled differential equation resulting from the stationary condition of the energy functional of the non-relativistic Hamiltonian (Fischer et al. 2016). Once radial orbitals have been obtained, Breit–Pauli configuration interaction (CI) calculations can be performed where the wave function is expanded in $LS\ J$-coupled CSFs:

$$\Psi(\gamma LS\ J) = \sum_j c_j \Phi(\gamma_j L_j S_j J). \tag{2}$$

In the CI calculation the expansion coefficients, c_j, are obtained by diagonalizing the Hamiltonian interaction matrix with respect to the Breit–Pauli operators. This is the intermediate coupling or $LS\ J$ approximation. If the interaction matrix is ordered according to LS terms the interaction has a block structure. Diagonal blocks represent interaction within CSFs of a given LS and off-diagonal blocks between CSFs of different LS terms. If off-diagonal interactions occur for a specific J we say that the LS terms interact and as a result of this interaction the terms mix in the wave function expansion.

In the fully relativistic multiconfiguration Dirac-Hartree-Fock (MCDHF) approach the wave function Ψ for a state labelled γJ is expanded in terms of jj-coupled CSFs:

$$\Psi(\gamma J) = \sum_j c_j \Phi(\gamma_j J). \tag{3}$$

The CSFs, $\Psi(\gamma J)$, are constructed from products of relativistic one-electron spin orbitals. The radial orbitals and the expansion coefficients of the CSFs are determined by iteratively solving a set of coupled differential equations resulting from the stationary condition of energy functional of the relativistic Dirac-Coulomb Hamiltonian (Grant 2007; Fischer et al. 2016). Once the radial orbitals have been obtained, relativistic configuration interaction (RCI) calculations can be performed where the Breit interaction and quantum electrodynamic (QED) effects can be added to the Hamiltonian. Relativistic wave functions are given in terms

Table 1. Summary of ions, the number of computed energy levels $N_{\rm cal-levels}$, and the number of Landé g-factors in NIST $N_{{\rm NIST}-g_J}$.

Ions	$N_{\rm cal-levels}$	$N_{{\rm NIST}-g_J}$	Ions	$N_{\rm cal-levels}$	$N_{{\rm NIST}-g_J}$	Ions	$N_{\rm cal-levels}$	$N_{{\rm NIST}-g_J}$
B II	100	0	Si I	168	0	Ar IV	103	0
C I	100	3	Si II	56	0	Ca I	45	0
C II	69	0	Si III	106	0	Ti II	99	15
C III	114	0	Si IV	45	0	Zr III	88	0
C IV	53	0	P II	106	76	Sn II	22	1
Al I	28	0	S II	134	0			
Al II	78	0	Cl III	87	0			

of jj-coupled CSFs. In order to have a labelling that is consistent with the one from the intermediate coupling approximation, CSFs are transformed from jj-coupling to LS J-coupling using the methods developed by Gaigalas et al. (2003, 2017).

2.2. Zeeman effect

The Zeeman effect is caused by the interaction between the magnetic moment of the atom and an external magnetic field. The operator representing the interaction is given by

$$\mathcal{H}_M = -\boldsymbol{\mu}\cdot\boldsymbol{B}, \tag{4}$$

where $\boldsymbol{\mu}$ is the magnetic moment of the electrons and $\boldsymbol{B}$ is the magnetic field. If the external magnetic field is weak such that the magnetic interaction energy is small compared to the fine structure separations, the interaction can be treated in first-order perturbation theory with the wave functions from the Breit–Pauli approximation or from the fully relativistic theory as zero-order functions.

In the Breit–Pauli approximation the magnetic moment can be written as

$$\boldsymbol{\mu} = -\mu_{\rm B}(\mathbf{L} + g_s\mathbf{S}), \tag{5}$$

where $\mu_{\rm B}$ is the Bohr magneton and $g_s \approx 2.00160$ is the g-factor of the electron spin corrected for QED effects. Using the Wigner–Eckart theorem to relate the matrix elements of $\mathbf{L} + g_s\mathbf{S}$ with the matrix element of $\mathbf{J}$, it can be shown that the magnetic moment is proportional to $\mathbf{J}$, i.e.

$$\mu_{\rm B}(\mathbf{L} + g_s\mathbf{S}) = \mu_{\rm B} g_{\gamma J}\mathbf{J}, \tag{6}$$

where the factor of proportionality, $g_{\gamma J}$, is the Landé g-factor. Choosing the direction of the external field as the z-direction the operator for the interaction can, using tensor-operator notation, be written as

$$\mathcal{H}_M = \mu_{\rm B}\left(\mathbf{L}_0^{(1)} + g_s\mathbf{S}_0^{(1)}\right)B = \mu_{\rm B} g_{\gamma J}\mathbf{J}_0^{(1)}B. \tag{7}$$

Inserting the wave function expansion from Eq. (2) and computing the reduced matrix elements of the interaction gives the Landé g-factor in intermediate coupling, i.e.

$$g_{\gamma J} = \sum_{i,j} c_i c_j \frac{\langle \gamma_i L_i S_i J\|\mathbf{L}^{(1)} + g_s\mathbf{S}^{(1)}\|\gamma_j L_j S_j J\rangle}{\sqrt{J(J+1)(2J+1)}}. \tag{8}$$

The matrix elements between the LS J-coupled CSFs can be analytically evaluated to give

$$\frac{\langle \gamma LS\ J\|\mathbf{L}^{(1)} + g_s\mathbf{S}^{(1)}\|\gamma' L' S' J\rangle}{\sqrt{J(J+1)(2J+1)}} = \delta_{\gamma\gamma'}\delta_{LL'}\delta_{SS'} g_J(LS), \tag{9}$$

where

$$g_J(LS) = 1 + (g_s - 1)\frac{J(J+1) + S(S+1) - L(L+1)}{2J(J+1)} \tag{10}$$

is the Landé g-factor in pure LS-coupling (Cowan 1981). Summing up the contributions from the different LS terms, we have

$$g_{\gamma J} = \sum_{LS} w(LS) g_J(LS), \tag{11}$$

where $w(LS)$ is the accumulated squared expansion coefficients for the CSFs with the specified LS term (Jönsson & Gustafsson 2002). The set of $w(LS)$ determine the LS J-composition of the wave function. The Landé g-factor in intermediate coupling thus provides a valuable probe of the coupling conditions in the atom (Fawcett 1990). To summarize, the full sum in Eq. (11) gives the Landé g-factor, $g_{\gamma J}$, in the intermediate coupling approximation. Truncating the sum to a single dominating LS term, often the one used to label the state, gives the Landé g-factor, $g_J(LS)$, in pure LS-coupling.

In the relativistic theory the interaction between the magnetic moment of the atom and an external field can be written as

$$\mathcal{H}_M = \frac{1}{2}\boldsymbol{N}\cdot\boldsymbol{B}, \tag{12}$$

where

$$N_q^{(1)} = -\sum_{j=1}^{N} i\sqrt{\frac{8\pi}{3}} r_j \boldsymbol{\alpha}_j \cdot Y_{1q}^{(0)}(\hat{r}_j) \tag{13}$$

is an operator of the same tensorial form as the magnetic dipole hyperfine operator (Cheng & Childs 1985). Just as in the Breit–Pauli approximation, we express the operator $\mathcal{H}_M$ in terms of $\mathbf{J}$ and the Landé g-factor, i.e.

$$\mathcal{H}_M = \frac{1}{2}\boldsymbol{N}_0^{(1)}B = \mu_{\rm B} g_{\gamma J}\mathbf{J}_0^{(1)}B. \tag{14}$$

Inserting the wave function expansion from Eq. (3) and evaluating the matrix elements of the interaction gives

$$g_{\gamma J} = \sum_{i,j} c_i c_j \frac{1}{2\mu_{\rm B}} \frac{\langle \gamma_i J\|\boldsymbol{N}^{(1)}\|\gamma_j J\rangle}{\sqrt{J(J+1)(2J+1)}}. \tag{15}$$

In the relativistic Dirac theory the electron g-factor is exactly 2. The QED corrections to this factor lead to a correction of the Landé g-factor. Defining the operator $\Delta\boldsymbol{N}$ by

$$\Delta\boldsymbol{N}_q^{(1)} = \sum_{j=1}^{N} \frac{g_s - 2}{2}\beta_j \boldsymbol{\Sigma}_{qj}, \tag{16}$$

the correction to the Landé g-factor is given by

$$\Delta g_{\gamma J} = \sum_{i,j} c_i c_j \frac{(g_s - 2)}{2} \frac{\langle \gamma_i J\|\Delta\boldsymbol{N}^{(1)}\|\gamma_j J\rangle}{\sqrt{J(J+1)(2J+1)}}. \tag{17}$$

3. Computational scheme

The accuracy of the computed Landé g-factors depends on the quality of the wave functions. From Eq. (11) we see that the g-factors require the mixing of LS-terms in the wave functions to be accurately determined (Fischer et al. 2004). This in turn depends on the CSFs expansions, what electron correlation effects are captured, and how well the resulting wave functions reproduce measured energy separations. For the studied atoms and ions the CSF expansions, aimed at producing accurate energies, are based on the multireference-single-double (MR-SD) approach (Fischer et al. 2016). In the MR-SD approach, the CSF expansions are obtained first by defining a set of important configurations referred to as the MR and then by allowing SD substitutions, according to some rules, of the orbitals in the MR configurations to orbitals in an active set (AS) (see Olsen et al. 1988; Sturesson et al. 2007; Fischer et al. 2016). Depending on the rules, substitutions for the CSF expansion will account for valence–valence (VV), core–valence (CV), and core–core (CC) electron correlation effects. The CSF expansions are systematically enlarged by increasing the active set along with the MR. A number of studies show that expansions accounting for VV and CV effects and based on reasonably large MR and active orbital sets often are sufficient for reproducing energy separations with high accuracy (Jönsson et al. 2017). The Breit interaction and leading QED effects (e.g. vacuum polarization and self-energy) can be accounted for in the following RCI calculations.

The computational schemes, as well as the evaluation of the wave functions and atomic data for each atomic system, are described in detail in Wang et al. (2018) (for B II), Papoulia et al. (2019a) (for C III-IV), Papoulia et al. (2019b) (for Al I–II), Pehlivan Rhodin et al. (2019) (for Si I–II), Atalay et al. (2019) (for Si III-IV), Rynkun et al. (2019a) (for P II), Rynkun et al. (2019b) (for S II, Cl III and Ar IV), and Rynkun et al. (2020) (for Zr III). The corresponding manuscripts of C I-C IV by Li et al., Ti II by Li et al., and Sn II by Atalay et al. (in prep.). The ions, as well as the details of the computational schemes and correlation effects (e.g. targeted configuration states, MR for RCI calculations, definition of core orbitals, correlation model for final RCI calculations, AS, and the number of generated CSFs) are summarized in Table 2.

All calculations of the wave functions were done using the MCDHF and RCI programs (Grant 2007; Fischer et al. 2016), which are parts of general relativistic atomic structure package GRASP2K (Jönsson et al. 2013; Fischer et al. 2019). The evaluation of the Landé g-factors was then done with the HFSZEEMAN programs (Andersson & Jönsson 2008; Li et al. 2020).

4. Evaluation of data

The accuracy of the Landé g-factors is to a large extent determined by the accuracy of the energy separations. In this section we evaluate the accuracy of the calculated energy levels by comparing them with the NIST recommended data. We then present the results for the Landé g-factors, $g_{\gamma J}$, and compare them with the Landé g-factors in pure LS-coupling, $g_J(LS)$. Finally, we compare the Landé g-factors with values from Kurucz's atomic database (Kurucz 2017).

4.1. Energy levels

The computed excitation energies and wave function composition in LS-coupling of the targeted atomic states in the B II, C I–IV, Al I–II, Si I–IV, P II, S II, Cl III, Ar IV, Ca I, Ti II, Zr III, and Sn II ions are displayed in Tables 5–23, respectively, and are available at the CDS. In the calculations the labelling of the eigenstates is determined by the LS J-coupled CSF with the largest coefficient in the expansion resulting from the transformation from jj-coupling to LS J-coupling using the methods by Gaigalas et al. (2017).

One of the quality indicators of calculations is the ability to reproduce the energy structure. Therefore, the accuracy of the wave functions from the calculations can be evaluated by comparing the calculated energy levels with data from the NIST database (Kramida et al. 2019). Here we define the average percentage difference between the present calculations and NIST as "Av. accuracy" to indicate the accuracy of the calculations. In Table 3 a summary of the Av. accuracy is presented for the targeted atoms and ions. As seen from Table 3, all energies are in very good agreement with the NIST recommended values. In particular, the Av. accuracy values are less than 0.1%; they are 0.089%, 0.088%, 0.044%, 0.004%, 0.05%, and 0.09%, respectively, for the Be II, C II–IV, Si III, and Si IV ions. The Av. accuracy values are less than 0.68% for C I, Al I–II, Si I–II, P II, S II, Cl III, Ar IV, Ca I, Zr III, and Sn II. For Ti II the average difference is larger, about 1.06%. The excellent agreement of the excitation energies with the NIST recommended values allows us to infer that the corresponding wave functions are very accurate (see the references given in Sect. 3 for each atom or ion for more details on how to estimate the accuracy.)

As we have already discussed, the Landé g-factor depends on the mixing of different LS terms, which in turn depends on the separation of these terms. The accuracy of the energy separation of the terms is thus a more proper measure of the accuracy of the Landé g-factors than the excitation energies. To evaluate the accuracy of the energy separation of the terms, we define a new average accuracy parameter $\overline{\mathrm{d}E_\mathrm{S}}$ by (i) classifying the states into different blocks by J-values and parity, one for each symmetry block; (ii) computing the energy separation relative to the lowest state of each block, $E_\mathrm{S} = E_i - E_\mathrm{min}$, where E_i is the excitation energy and E_min is the lowest energy of each block; (iii) computing the relative difference with the NIST values, $\mathrm{d}E_\mathrm{S} = \frac{|E_\mathrm{S} - E_{S-\mathrm{NIST}}|}{E_\mathrm{S}}$, where $E_{S-\mathrm{NIST}}$ is the energy separation from the NIST database; and (iv) averaging the difference, $\overline{\mathrm{d}E_\mathrm{S}} = \frac{\sum \mathrm{d}E_\mathrm{S}}{N_{E_\mathrm{S}}}$, where N_{E_S} is the number of the energy separations. The results are shown in Table 4 for even and odd states. Generally, the uncertainties of the energy separations are larger than those of the excitation energies, especially when the energy separations are very small. However, for most of the levels, $\mathrm{d}E_\mathrm{S}$ is well below 1%. For a few levels for which E_S is small, $\mathrm{d}E_\mathrm{S}$ is higher than 5% and these data have been excluded to obtain the average difference values shown in Table 4 (one level for C I, one for C III, one for Si I, one for Si II, one for Si III, one for Ar IV, one for Ca I, and five levels for Ti II). Table 4 shows that the average uncertainty $\overline{\mathrm{d}E_\mathrm{S}}$ is well below 1%, except for even states of Al I; odd states of Si I, Ca I, Ti II, Zr III; and even states of Sn II. For these levels the relative difference is between 1% and 2%. The good agreement of the energy separations of the terms with the NIST data confirms the reliable values of the mixing between the relativistic CSFs, which is a good indicator of the quality of the produced Landé g-factors.

4.2. Landé g-factors

Tables 5–23 display the Landé g-factors, $g_{\gamma J}$, for the lowest states (shown in Table 1) in the B II, C I–IV, Al I–II, Si I–IV, P II, S II, Cl III, Ar IV, Ca I, Ti II, Zr III, and Sn II ions, respectively.

Table 2. Summary of the computational schemes of B II, C I–IV, Al I–II, Si I–IV, P II, S II, Cl III, Ar IV, Ca I, Ti II, Zr III, and Sn II.

Configurations	MR-RCI	Core orbitals	Correlation	AS	$N_{\rm NCFs}$
	B II [(1)], $N_{\rm levels}$ = 100				
$2s^2$,$2p^2$, {2s,2p}nl ($n \le 6, l \le 5$)	$2s^2$,$2p^2$, {2s,2p}nl ($n \le 6, l \le 5$)	1s	VV + CV + CC (1s)	{11s,11p,11d,11f, 11g,11h,11i,11k}	e: 777 325 o: 800 410
	C I, $N_{\rm levels}$ = 100				
$2s2p^3$ $2s^22p\{n_1s,n_2p,n_3d,4f\}$ ($3 \le n_1 \le 6, 2 \le n_2 \le 5, 3 \le n_3 \le 5$)	$2s2p^3$ $2s^22p\{n_1s,n_2p,n_3d,4f\}$ ($3 \le n_1 \le 6, 2 \le n_2 \le 6, 3 \le n_3 \le 5$) $2p^3\{n_1s,n_2p,n_3d\}$ ($3 \le n_1 \le 6, 3 \le n_2 \le 5, 3 \le n_3 \le 6$) $2s2p^2\{3s,3p,4p,6p,6d,7s\}$ $2s2p\{n_1s,n_2p,n_3d,4f\}6d$ ($3 \le n_1 \le 6, 3 \le n_2 \le 5, 3 \le n_3 \le 5$)	1s	VV + CV (1s)	{11s,10p,10d,9f, 7g,6h}	e: 14 941 842 o: 15 572 953
	C II, $N_{\rm levels}$ = 69				
$2s^2nl(n \le 6, l \le 4)$ $2s^27l(l \le 3)$ $2s2p^2$, $2p^3$, 2s2p3s, 2s2p3p	$2s2p^2$, $2s^2\{n_1s,n_2p,n_3d,n_4f,n_5g\}$ ($3 \le n_1 \le 7, 2 \le n_2 \le 8, 3 \le n_3 \le 7$ $4 \le n_4 \le 7, 5 \le n_5 \le 6$) $2p^3$, $2p^2\{n_1s,n_2p,n_3d,n_4f,n_5g\}$ ($3 \le n_1 \le 7, 4 \le n_2 \le 7, 3 \le n_3 \le 7$ $4 \le n_4 \le 7, 5 \le n_5 \le 6$) $2s2p\{3s,4s,8s,3p,3d,4d,5d,6d,8d\}$ $2s3s\{3p,8p\}$	1s	VV + CV (1s)	{13s,13p,13d,13f, 10g,8h}	e: 6 623 511 o: 4 768 481
	C III [(2)], $N_{\rm levels}$ = 114				
$2snl(n \le 7, l \le 4)$ $2p^2$, 2p{3s,3p,3d}	$2snl$ ($n \le 7, l \le 4$) $2p^2$, 2p{3s,3p,3d}	1s	VV + CV (1s)	{12s,12p,12d,12f, 11g,8h}	e: 1 578 620 o: 1 274 147
	C IV [(2)], $N_{\rm levels}$ = 53				
$1s^2nl$ ($n \le 8, l \le 4$) $1s^26h$	$1s^2nl$ ($n \le 8, l \le 4$) $1s^26h$	1s	CV + CC (1s)	{14s,14p,14d,12f,12g, 8h,7i}	e: 1 077 872 o: 1 287 706
	Al I [(3)], $N_{\rm levels}$ = 28				
$3s3p^2$, $3s^2\{n_1s,n_2p,n_3d,n_4f,5g\}$ ($4 \le n_1 \le 6, 3 \le n_2 \le 6, 3 \le n_3 \le 6$, $4 \le n_4 \le 5$)	$3s3p^2$, $\{3s^2,3p^2\}\{n_1s,n_2p,n_3d,n_4f,5g\}$ ($4 \le n_1 \le 6, 3 \le n_2 \le 6, 3 \le n_3 \le 6$, $4 \le n_4 \le 5$)	1s,2s,2p	VV + CV (2p)	{12s,12p,12d,11f, 11g,10h}	e: 4 362 628 o: 2 889 385
	Al II [(3)], $N_{\rm levels}$ = 78				
$3s^2$, $3p^2$, 3s6h, 3p3d $3s\{n_1s,n_2p,n_3d,n_4f\}$ ($4 \le n_1 \le 7, 3 \le n_2 \le 7, 3 \le n_3 \le 6$, $4 \le n_4 \le 6$)	$3s^2$, $3p^2$, 3s6h, 3p3d $3s\{n_1s,n_2p,n_3d,n_4f\}$ ($4 \le n_1 \le 7, 3 \le n_2 \le 7, 3 \le n_3 \le 6$, $4 \le n_4 \le 6$)	1s,2s,2p	VV + CV (2s,2p)	{13s,13p,12d,12f,12g, 8h,7i}	e: 911 795 o: 1 269 797
	Si I [(4)], $N_{\rm levels}$ = 168				
$3s^23p^2$, $3s3p^3$, $3s^23p5g$ $3s^23p\{n_1s,n_2p,n_3d,n_4f\}$ ($4 \le n_1 \le 8, 4 \le n_2 \le 7, 3 \le n_3 \le 6$, $4 \le n_4 \le 6$)	$3s^23p^2$, $3s3p^3$, $3p^4$, $3s^23p5g$, $3s3p^23d$, $3p^37d$, $3s3p7d^2$, $3s^23p3d$, $3p^35g$, $\{3s^23p,3p^3,3s3p3d\}\{n_1s,n_2p,n_3d,n_4f\}$ ($4 \le n_1 \le 8, 4 \le n_2 \le 7, 3 \le n_3 \le 6$ $4 \le n_4 \le 6$), 3s3p3d5g	1s,2s,2p	VV + CV (2s,2p)	{13s,12p,12d,11f,10g, 9h,7i} for VV {9p,7d,6f,5g} for CV	e: 8 789 575 o: 9 097 389
	Si II [(4)], $N_{\rm levels}$ = 56				
$3s3p^2$, 3s3p3d, 3s3p4s, $3s^2$5g,6g} $3s^2\{n_1s,n_2p,n_3d,n_4f\}$ ($4 \le n_1 \le 8, 3 \le n_2 \le 7, 3 \le n_3 \le 7$, $4 \le n_4 \le 7$)	$3s3p^2$, 3s3p3d, 3s3p4s, $3s^2\{5g,6g\}$ $3s^2\{n_1s,n_2p,n_3d,n_4f4\}$ ($4 \le n_1 \le 8, 3 \le n_2 \le 7, 3 \le n_3 \le 7$, $4 \le n_4 \le 7$)	1s,2s,2p	VV + CV (2s,2p)	{13s,12p,12d,11f,10g, 9h,7i} for VV {9p,7d,6f,5g} for CV	e: 5 267 943 o: 6 582 233
	Si III [(5)], $N_{\rm levels}$ = 106				
$3s^2$, $3p^2$, 3p4s, 3p4p, $3s\{n_1s,n_2p,n_3d,n_4f,n_5g\}$ ($4 \le n_1 \le 7, 3 \le n_2 \le 7, 3 \le n_3 \le 7$, $4 \le n_4 \le 7, 5 \le n_5 \le 7$) 3pnd ($3 \le n_2 \le 4$)	$3s^2$, $3p^2$, 3p4s, 3p4p, $3s\{n_1s,n_2p,n_3d,n_4f,n_5g\}$ ($4 \le n_1 \le 9, 3 \le n_2 \le 9, 3 \le n_3 \le 8$, $4 \le n_4 \le 8, 5 \le n_5 \le 8$) 3pnd ($3 \le n_2 \le 4$)	1s,2s,2p	VV + CV (2s,2p)	{13s,13p,12d,12f,12g, 9h}	e:1 401 150 o: 1 760 209
	Si IV [(5)], $N_{\rm levels}$ = 45				
$2s^22p^6nl$ ($n \le 7, l \le 6$)	$2s^22p^6nl$ ($n \le 9, l \le 6$)	1s,2s,2p	CV + CC (2s,2p)	{13s,13p,13d,12f,12g, 12h,12i}	e: 995 020 o: 993 501

Notes. $N_{\rm levels}$ is the number of the targeted levels computed in this work. Configuration denotes the targeted configuration states. MR-RCI denotes multireference for relativistic configuration interaction calculations. Core orbitals denotes core orbitals defined in the calculations. Correlation denotes correlation effects included in the calculation. The orbitals included in the CV and CC correlation effects are shown in parentheses and the remaining core orbitals define an inactive closed core. AS denotes active set of orbitals; $N_{\rm CSFs}$ is the number of generated configuration state functions for the relativistic configuration interaction calculations.

References. (1) Wang et al. (2018); (2) Papoulia et al. (2019a); (3) Papoulia et al. (2019b); (4) Pehlivan Rhodin et al. (2019); (5) Atalay et al. (2019); (6) Rynkun et al. (2019a); (7) Rynkun et al. (2019b); (8) Rynkun et al. (2020).

Table 2. continued.

Configurations	MR-RCI	Core orbitals	Correlation	AS	$N_{\rm NCFs}$
	P II [6], $N_{\rm levels}$ = 106				
$3s^23p^2$, $3s3p^23d$, $3s3p^3$, $3s^23p\{n_1s,n_2p,n_3d,n_4f\}$ $(4 \le n_1 \le 6, 4 \le n_2 \le 6, 3 \le n_3 \le 5, 4 \le n_4 \le 5)$	$3s^23p^2$, $3s3p^23d$, $3s3p^3$, $3s^23d^2$, $3p^4$, $3s^23d7d$, $3s3p^27d$, $3s3p^24p$, $3p^37d$, $3s^23p\{n_1s,n_2p,n_3d,n_4f\}$ $(4 \le n_1 \le 7, 4 \le n_2 \le 6, 3 \le n_3 \le 7, 4 \le n_4 \le 5)$ $3p^3\{n_1s,n_2p,n_3d,n_4f\}$ $(4 \le n_1 \le 7, 4 \le n_2 \le 6, 3 \le n_3 \le 7, 4 \le n_4 \le 5)$	1s,2s,2p	VV + CV (2p)	{12s,11p,11d,10f,9g, 7h,7i}	e: 5 954 032 o: 4 815 663
	S II [7], $N_{\rm levels}$ = 134				
$3s3p^4$, $3s^23p^3$, $3s3p^33d$ $3s^23p^2\{n_1s,n_2p,n_3d,n_4f\}$ $(4 \le n_1 \le 5, 4 \le n_2 \le 5$ $3 \le n_3 \le 4, n_4 = 4)$	$3s3p^4$, $3s^23p^3$, $3s3p^33d$, $3p^5$ $3s^23p^2\{n_1s,n_2p,n_3d,n_4f\}$ $(4 \le n_1 \le 5, 4 \le n_2 \le 5$ $3 \le n_3 \le 5, n_4 = 4)$ $3p^4\{3d,4s,4p,4d,4f,5s,5p\}$ $3s3p^23d\{3d,4s,4p,4d,4f,5s,5p\}$	1s,2s,2p	VV + CV (2p)	{9s,9p,9d,8f,8g,8h,8i} {6s,6p,5d,5f} for S from 2p	e: 6 220 422
	Cl III [7], $N_{\rm levels}$ = 87				
$3s3p^4$, $3s^23p^3$, $3s3p^33d$, $3p^5$ $3s^23p^2\{3d,4s,4p,4d\}$	$3s3p^4$, $3s^23p^3$, $3s3p^33d$, $3p^5$ $3p^4\{3d,4p\}$, $3s3p^34s$, $3s3p^23d^2$ $3s3p^23d\{4s,4p,4d\}$, $3s^23p3d^2$	1s,2s,2p	VV + CV (2p)	{9s,9p,9d,8f,8g,8h,8i} {6s,6p,5d,5f} for S from 2p	e: 6 466 816 o: 4 111 005
	Ar IV [7], $N_{\rm levels}$ = 103				
$3s3p^4$, $3s^23p^3$, $3s3p^33d$, $3p^5$ $3s^23p^2\{3d,4s,4p\}$	$3s3p^4$, $3s^23p^3$, $3s3p^33d$, $3p^5$ $3s^23p^2\{3d,4s,4p,4d,4f\}$, $3p^43d$ $3s3p^23d\{3d,4s,4p\}$, $3s3d^24s$, $3s^23d^3$ $3s^23p3d^2$, $3s3p^34s$, $3p^44p$, $3p^33d^2$	1s,2s,2p	VV + CV (2p)	{9s,9p,9d,8f,8g,8h,8i} {7s,6p,6d,6f,5g} for S from 2p	e: 4 946 496 o: 7 329 546
	Ca I, $N_{\rm levels}$ = 45				
$4s^2$, $4p^2$, $3d\{4s,4p\}$, $4s\{4p,4d,4f,5s,5p,6s,6p\}$	$4s^2$, $4p^2$, $3d^2$ $4s\{5s,6s,4p,5p,6p,4d,5d,4f\}$ $4p\{5p,7p,4d,5d\}$ $3d\{4s,5s,4p,5p,4d,5d\}$	1s,2s,2p, 3s,3p	VV + CV + CC (3s,3p)	{10s, 10p, 8d, 8f, 8g, 6h} {10s,10p,8d} for CC	e: 2 916 533 o: 3 021 057
	Ti II, $N_{\rm levels}$ = 99				
$3d^2\{4s,4p\}$, $3d^3$, $3d4s^2$ $3d4s4p$	$3d^2\{4s,4p,4d\}$, $3d^3$, $3d\{4s^2,4p^2,4d^2\}$ $3d4s\{4p,4d,5s\}$, $4s^2\{4p,4d\}$, $4s\{4p^2,4d^2\}$ $4s4p4d$, $3d4s5p$, $3d4p4d$, $4p4d^2$ $3p^4\{3d^44s,3d^5,3d^34s^2,3d^44p,3d^34s4p\}$	1s,2s,2p, 3s,3p	VV + CV + CC (3s,3p)	{8s,8p,8d,8f,8g,8h,7i} {8s,8p,8d} for CC	e: 14 089 101 o: 15 573 967
	Zr III [8], $N_{\rm levels}$ = 88				
$4d^2$, $5s^2$, $5p^2$, $5s5p$, $4d\{4f,5s,5p,5d,6s,6p\}$	$4d^2$, $5s^2$, $5p^2$, $5p5d$, $5s\{5p,5d\}$, $4d\{4f,5s,5p,5d,6s,6p,6d\}$	1s,2s,2p,3s, 3p,4s,4p	VV + CV + CC (4s,4p)	{11s,11p,10d,9f,7g,7h}	e: 14 255 953 o: 16 514 844
	Sn II, $N_{\rm levels}$ = 22				
$5s^2\{4f,5p,5d,6s,6p,6d,7s,7p\}$, $5s5p^2$	$5s^2\{4f,5p,5d,6s,6p,6d,7s,7p,$ $7d,8s,8p\}$, $5s5p^2$	1s,2s,2p,3s, 3p,4s,4p,4d	VV + CV (4s, 4p,4d)	{14s,14p,13d,10f,10g, 8h,8i}	e: 1 329 994 o: 674 998

Table 3. Comparison of computed energy levels in the present work with data from the NIST database.

Ions	Av. accuracy (%)	Ions	Av. accuracy (%)	Ions	Av. accuracy (%)
B II	0.089	Si I	0.25	Ar IV	0.21
C I	0.26	Si II	0.16	Ca I	0.68
C II	0.088	Si III	0.05	Ti II	1.06
C III	0.044	Si IV	0.09	Zr III	0.57
C IV	0.0044	P II	0.19	Sn II	0.22
Al I	0.60	S II	0.22		
Al II	0.17	Cl III	0.18		

In Table A.1, the computed $g_{\gamma J}$ values are compared with the available experimental values for C I (Lott et al. 1966), C III (Lott et al. 1966), P II (Li 1972), Si I (Lott et al. 1966), Si III (Lott et al. 1966), Si IV (Lott et al. 1966), Ti II (Moore 1949), and Sn II (David et al. 1980). The corresponding $g_J(LS)$ values are also displayed in the third column for a comparison. From Eq. (11) it is clear that there is a significant change in $g_{\gamma J}$ only when there is a strong mixing between terms with greatly different $g_J(LS)$ values. For C I, C III, Si I, Si III, Si IV, and Sn II the relative differences between $g_{\gamma J}$ and $g_J(LS)$ are rather small, within 0.7%, meaning that the mixing between terms is either small or occurs between terms with nearly the same $g_J(LS)$,

Table 4. Comparison of computed energy separations with NIST data.

Ions	$\overline{dE_S}$ (%)		Ions	$\overline{dE_S}$ (%)		Ions	$\overline{dE_S}$ (%)	
	Even	Odd		Even	Odd		Even	Odd
B II	0.24	0.28	Si I	0.35	1.37 (*)	Ar IV	0.41 (*)	0.23
C I	0.42	0.95 (*)	Si II	0.30 (*)	0.24	Ca I	1.94	1.29 (*)
C II	0.23	0.49	Si III	0.18 (*)	0.89 (*)	Ti II	1.81 (*)	1.55 (*)
C III	0.059 (*)	0.14	Si IV	0.062	0.050	Zr III	0.89	1.01
C IV	0.0051	0.0043	P II	0.23	0.82	Sn II	1.17	0.22
Al I	1.47	0.46	S II	0.82	0.45			
Al II	0.24	0.47	Cl III	0.44	0.31			

Notes. (*)The values are obtained by excluding the levels with dE_S higher than 5%.

which will not change $g_{\gamma J}$ appreciably (Fischer et al. 2004). The experimental values for the C and Si ions, displayed in the last column, are obtained from observations of atomic Zeeman patterns using strong pulsed magnetic fields (Lott et al. 1966). For most of the levels the computed and the experimental $g_{\gamma J}$-values agree within the experimental errors, i.e. 1%−3% for C I, C III, Si I, and Si III, and a factor of two higher for Si IV due to the broad spectra lines. The good agreement between theory and experiment, and with the $g_J(LS)$, indicates that these states of C I, C III, Si I, Si III, and Si IV are well described in LS-coupling. One exception is level 7 of Si IV for which the LS-composition (see Table 15) is dominated by one term, giving $g_{\gamma J} = 0.66583$ in close agreement with the value $g_J(LS) = 0.66667$ in pure LS-coupling. These values differ by more than 8% from the measured value $g_{\gamma J} = 0.72$. Since there is excellent agreement with the NIST recommended data, for the excitation energies and for energy separations, we are confident in our value and suggest a re-measurement for this level.

Some states of P II are strongly mixed in LS-coupling. Out of the 76 levels in P II for which experimental Landé g-factors are available, 23 levels have relative differences between $g_{\gamma J}$ and $g_J(LS)$ greater than 3%. We especially note a 44% difference for levels 27 and 50, a 30% difference for levels 29 and 54, a 29% difference for level 94, and a 22% difference for level 57. The departure from LS-coupling is quantified in Table 16, for example level 27, labelled $^3D^\circ_1$, has the composition 45% $3s^2\,3p\ ^2P\,3d\ ^3D^\circ_1$, 26% $3s^2\,3p\ ^2P\,3d\ ^3P^\circ$, and 8% $3s\ ^2S\,3p^3(^2_3D)\ ^3D^\circ$. The $g_J(LS)$ of $^3D_1$ has the relatively small value of 0.50000, whereas the value for $^3P_1$ is 1.50000, and so the mixing results in an appreciable increase in the smaller value. The experimental Landé g-factors of P II are from measurements of the Zeeman effect using the electrodeless discharge tubes operated in a given magnetic field (Li 1972). Comparisons between the computed $g_{\gamma J}$ and measured values show that there is a good agreement for most of the levels within the experimental uncertainties of 0.01 (0.02 for most of the $g_{\gamma J}$ values of 3p5d levels), except for levels 27 and 29 for which the relative difference is about 5%, and for levels 49 and 51 for which the relative difference is about 4%.

For Ti II there are 15 levels for which experimental data are available. Of these 15 levels, 7 have relative differences between $g_{\gamma J}$ and $g_J(LS)$ greater than 1%, especially 18% for level 18 and 23% for level 57. From the LS-percentage composition shown in Table 21, level 18 has the composition 61% $3d^3(^2_3P)\ ^2P_{1/2}$, 26% $3d^2(^3_2P)\ ^3P\,4s\ ^2P_{1/2}$, and 3% $3d^2(^3_2P)\ ^3P\,4s\ ^4P_{1/2}$. The $g_J(LS)$ for $^2P_{1/2}$ has a relatively small value of 0.66607, whereas the value for $^4P_{1/2}$ is 2.63809 and the mixing results in a 17% increase in the smaller value. Level 57 has the composition of 51% $3d^2(^1_2D)\ ^1D\,4p\ ^2D^\circ_{3/2}$, 29% $3d^2(^1_2D)\ ^1D\,4p\ ^2P^\circ$, and 5% $3d^2(^3_2P)\ ^3P\,4p\ ^2D^\circ$. The $g_J(LS)$ for $^2D_{3/2}$ has a relatively small value of 0.8, whereas the value for $^2P_{3/2}$ is 1.33333, and the mixing results in an appreciable change in the $3d^24p\ ^2D^\circ_{3/2}$ value to 0.98131. Compared with the NIST recommended Landé g-factors of Ti II (Corliss & Sugar 1979; Sugar & Corliss 1985; Saloman 2012), levels 18, 45, 56, and 57 have relative differences of 15%, 15%, 5%, and 23%, respectively. The suggested LS-percentage compositions are from the calculations of Huldt et al. (1982). The experimental g-values were determined by Catalán from the Zeeman patterns observed by King and Babcock and quoted by Russell (1927). They were published by Moore (1949). For level 18, NIST gives similar values of the leading compositions with present calculation, 62% $3d^3(^2_3P)\ ^2P_{1/2}$ and 24% $3d^2(^3_2P)\ ^3P\,4s\ ^2P_{1/2}$, but not for that of $3d^2(^3_2P)\ ^3P\,4s\ ^4P_{1/2}$, which mainly contributes to the changes in $g_{\gamma J}$. The same happens for level 45. The labelling of level 56 identifies the dominant component of the composition with 94% $3d^2(^3_2P)\ ^3P\,4p\ ^2S^\circ_{1/2}$, which indicates a good description in LS-coupling. The weak mixing results in $g_{\gamma J} = 1.99657$ in relative to $g_J(LS) = 2.00000$. However, NIST suggests 99% $^2S^\circ_{1/2}$, but gives an even larger $g_{\gamma J}$ value of 2.09. For level 57, NIST suggests 48% $3d^2(^1_2D)\ ^1D\,4p\ ^2D^\circ_{3/2}$ and 36% $3d^2(^1_2D)\ ^1D\,4p\ ^2P^\circ$ and $g_{\gamma J} = 1.21$ in relative to the computed value $g_{\gamma J} = 0.98131$. As stated in Russell (1927), due to the limitations inherent in old laboratory analyses, very few patterns have been resolved which resulted in large uncertainties of the observed g-values. It is highly desirable to redo the measurements by using the current high-resolution instruments and techniques. For level 3 of Sn II, LS-coupling is a good approximation and the computed $g_{\gamma J} = 2.65984$ agrees well with the measured value of 2.66085 within the experimental uncertainty of 5% (David et al. 1980).

In Fig. 1, we compare the computed $g_{\gamma J}$ values with $g_J(LS)$, and with available results in Kurucz's atomic database (Kurucz 2017) for all the atoms and ions presented in this work. The good agreement between $g_{\gamma J}$ and $g_J(LS)$ in B II, C II, C III, C IV, Al I, Al II, Si II, Si III, Si IV, and Ca I, indicates that these atoms and ions are well described in LS-coupling approximation. For some states of the rest of the atom and ions, the strong mixing of LS-terms results in large differences between $g_{\gamma J}$ and $g_J(LS)$ by >10%. Kurucz's atomic data (Kurucz 2017), which are widely adopted by the solar scientists for the spectropolarimetric modelling, are either taken from the experimental results or, when no experimental values are available, from semi-empirical values. From Fig. 1 we see that there is good agreement between

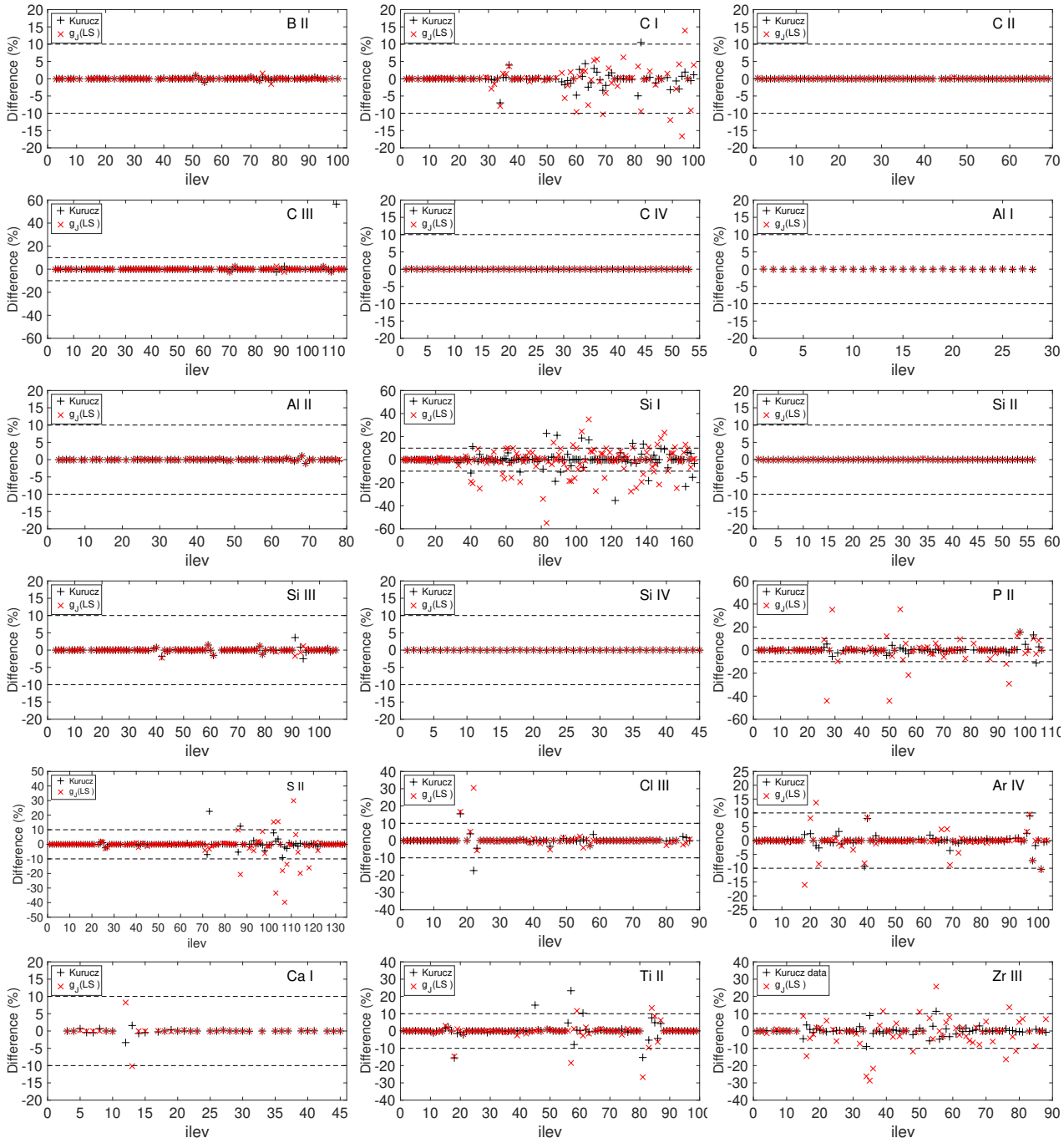

Fig. 1. Comparison of computed Landé g-factors, $g_{\gamma J}$, in the present work with values in LS-coupling, $g_J(LS)$ (red cross sign) and with Kurucz's data (black plus sign). Differences $((g_{\rm other}\text{-}g_{\gamma J})/g_{\gamma J})$ are given in percentage. The dashed lines indicate the −10% and 10% deviations.

the computed $g_{\gamma J}$ values and Kurucz's data, except for a number of energy levels in C III, Si I, Ti II, and Zr III with relative differences >10%. In Table A.2, we display all these states with a relative difference between $g_{\gamma J}$ and $g_J(LS)$ of more than 10%. Additionally, we present the $g_{\gamma J}$ values in the last column for comparison. Except for the levels of P II and level 18 and 57 of Ti II, for which the Kurucz's data are from experimental results (see discussion above), the others are semi-empirical determinations of the Landé g-factor in intermediate coupling. The computed $g_{\gamma J}$ using the fully relativistic MCDHF approach differ from the semi-empirical values by more than 10% for several cases, e.g. level 82 of C I; levels 40, 41, 68, 83, 138, and 144 of Si I; level 87 of S II; levels 18 and 22 of Cl III; and levels 18 and 101 of Ar IV. The data for Sn II are absent in Kurucz's database.

5. Summary

In the present work Landé g-factors are computed for the B II, C I–IV, Al I–II, Si I–IV, P II, S II, Cl III, Ar IV, Ca I, Ti II, Zr III, and Sn II ions, all of which are of astrophysical interest. The MCDHF and RCI methods, which are implemented in the general-purpose relativistic atomic structure package GRASP2K, are used in the present work. The accuracy of the present calculations is validated by extensive comparisons of the excitation energies and energy separations with the NIST

recommended data. All excitation energies are in good agreement with the NIST values. The Av. accuracy values are within 0.1%, 0.089%, 0.088%, 0.044%, 0.004%, 0.05%, and 0.09%, respectively, for the Be II, C II–IV, Si III, and Si IV ions, and are less than 0.68% for the C I, Al I–II, Si I–II, P II, S II, Cl III, Ar IV, Ca I, Zr III, and Sn II ions. For Ti II, the average difference is about 1.06%.

The Landé g-factor depends on the mixing of LS terms, which in turn, depends on the separation of these terms. The accuracy of the energy separations in each symmetry block is thus a more proper measure of the accuracy of the Landé g-factors than the excitation energies. The average accuracy of the energy separations is well below 1% except for even states of Al I; odd states of Si I, Ca I, Ti II, Zr III; and even states of Sn II, all of which show a relative difference of between 1% and 2%.

The computed $g_{\gamma J}$ values are compared with available experimental values, and with the values in pure LS-coupling. The differences with the values in LS-coupling are explained by analysing wave function LS-compositions. The observed and theoretical g-values differ by a small percentage in some cases, which may be due to the limitations in old laboratory analyses. It is highly recommended to redo the measurements for these cases. We summarize the levels with a difference of more than 10% between the $g_{\gamma J}$ and $g_J(LS)$ values, and make a comparison with the semi-empirical values from the Kurucz's database. The present calculations provide a substantial amount of critically evaluated Landé g-factors that are useful for modelling and diagnostics of astrophysical plasmas.

Acknowledgements. This work is supported by the Swedish research council under contracts 2015-04842 and 2016-04185. Betül Atalay acknowledges financial support from the Scientific and Technological Research Council of Turkey (TUBITAK) – BIDEB 2219 International Post-Doctoral Research Fellowship Program.

References

Andersson, M., & Jönsson, P. 2008, Comput. Phys. Commun., 178, 156
Atalay, B., Brage, T., Jönsson, P., & Hartman, H. 2019, A&A, 631, A29
Biémont, É., Palmeri, P., & Quinet, P. 2010, J. Phys. B: At. Mol. Opt. Phys., 43, 074010
Brage, T., Judge, P. G., Jönsson, P., & Edwards, D. P. 2000, ApJ, 540, 1114
Cheng, K. T., & Childs, W. J. 1985, Phys. Rev. A, 31, 2775
Corliss, C., & Sugar, J. 1979, J. Phys. Chem. Ref. Data, 8, 1
Cowan, R. D. 1981, The Theory of Atomic Structure and Spectra (Berkeley, CA: University of California Press)
David, D., Hamel, J., & Barrat, J.-P. 1980, Opt. Commun., 32, 241
Fawcett, B. C. 1990, Phys. Scr., 42, 173
Fischer, C. F., Jönsson, P., & Tachiev, G. 2004, Mol. Phys., 102, 1177
Fischer, C. F., Godefroid, M., Brage, T., Jönsson, P., & Gaigalas, G. 2016, J. Phys. B: At. Mol. Opt. Phys., 49, 182004
Fischer, C. F., Gaigalas, G., Jönsson, P., & Bieroń, J. 2019, Comput. Phys. Commun., 237, 184
Gaigalas, G., Žalandauskas, T., & Rudzikas, Z. 2003, At. Data Nucl. Data Tables, 84, 99
Gaigalas, G., Fischer, C. F., Rynkun, P., & Jönsson, P. 2017, Atoms, 5, 6
Grant, I. P. 2007, Relativistic Quantum Theory of Atoms and Molecules (New York: Springer)
Huldt, S., Johansson, S., Litzén, U., & Wyart, J.-F. 1982, Phys. Scr., 25, 401
Jönsson, P., & Gustafsson, S. 2002, Comput. Phys. Commun., 144, 188
Jönsson, P., Gaigalas, G., Bieroń, J., Fischer, C. F., & Grant, I. 2013, Comput. Phys. Commun., 184, 2197
Jönsson, P., Gaigalas, G., Rynkun, P., et al. 2017, Atoms, 5, 16
Judge, P. G. 2017, Can. J. Phys., 95, 847
Keil, S. L., Rimmele, T. R., & Wagner, J. 2009, Earth Moon Planets, 104, 77
Kramida, A., Ralchenko, Yu., Reader, J., & NIST ASD Team 2019, NIST Atomic Spectra Database (ver. 5.7.1), [Online]. Available: https://physics.nist.gov/asd [2020, February 11]. National Institute of Standards and Technology, Gaithersburg, MD
Kurucz, R. L. 2017, On-line Database of Observed and Predicted Atomic Transitions (Cambridge, MA: Harvard-Smithsonian Center for Astrophysics), http://kurucz.harvard.edu
Landi Degl'Innocenti, E. 1982, Sol. Phys., 77, 285
Landi Degl'Innocenti, E., & Landolfi, M. 2004, in Polarization in Spectral Lines (Dordrecht: Kluwer Academic Publishers), Astrophys. Space Sci. Lib., 307
Li, H. 1972, J. Opt. Soc. Am., 62, 1483
Li, W., Casini, R., del Pino Alemán, T., & Judge, P. G. 2017, ApJ, 848, 82
Li, W., Grumer, J., Brage, T., & Jönsson, P. 2020, Comput. Commun. Phys., 107211
Lott, S. H., Roos, C. E., & Ginter, M. L. 1966, J. Opt. Soc. Am., 56, 775
Martin, W. C., Zalubas, R., & Musgrove, A. 1985, J. Phys. Chem. Ref. Data, 14, 751
Moore, C. E. 1949, Atomic Energy Levels. 1949, Nat. Bur. Stand. (U.S.) Circ. 467, Vol. I, 309 pp.; 1952, Vol. II, 227 pp.; 1958, Vol. III, 245 pp.; 1971, Reprinted in Three Volumes as Nat. Stand. Ref. Data Ser., Nat. Bur. Stand. (U.S.), 35
Olsen, J., Roos, B. O., Jørgensen, P., & Jensen, H. J. A. 1988, J. Chem. Phys., 89, 2185
Papoulia, A., Ekman, J., Gaigalas, G., et al. 2019a, Atoms, 7, 106
Papoulia, A., Ekman, J., & Jönsson, P. 2019b, A&A, 621, A16
Pehlivan Rhodin, A., Hartman, H., Nilsson, H., & Jönsson, P. 2019, A&A, submitted
Russell, H. N. 1927, ApJ, 66, 283
Rynkun, P., Radžiūtė, L., Gaigalas, G., & Jönsson, P. 2019a, A&A, 622, A167
Rynkun, P., Gaigalas, G., & Jönsson, P. 2019b, A&A, 623, A155
Rynkun, P., Gaigalas, G., & Jönsson, P. 2020, A&A, 637, A10
Saloman, E. B. 2012, J. Phys. Chem. Ref. Data, 41, 013101
Sturesson, L., Jönsson, P., & Froese Fischer, C. 2007, Comput. Phys. Commun., 177, 539
Sugar, J., & Corliss, C. 1985, J. Phys. Chem. Ref. Data, 14
Verdebout, S., Naze, C., Jönsson, P., et al. 2014, At. Data Nucl. Data Tables, 100, 1111
Wang, K., Chen, Z. B., Zhang, C. Y., et al. 2018, ApJS, 234, 40

Appendix A: Additional tables

Table A.1. Comparison of computed Landé g-factors, $g_{\gamma J}$, with their LS-coupling values $g_J(LS)$ and experimental values (Exp.).

No.	State	$g_J(LS)$	$g_{\gamma J}$	Exp.
	C I [1]			
2	$2p^2(^3_2P)\ ^3P_1$	1.50000	1.50109	1.5010623(50)
3	$2p^2(^3_2P)\ ^3P_2$	1.50000	1.50107	1.5010469(50)
10	$2p\ ^2P\,3s\ ^1P^\circ_1$	1.00000	1.00007	0.97
	C III [1]			
5	$2s\ ^2S\,2p\ ^1P^\circ_1$	1.00000	0.99990	1.01
9	$2p^2(^1_2D)^1D_2$	1.00000	0.99991	1.01
	P II [2][3]			
7	$3s\ ^2S\,3p^3(^2_3D)\ ^3D^\circ_1$	0.50000	0.49910	0.504
8	$3s\ ^2S\,3p^3(^2_3D)\ ^3D^\circ_2$	1.16667	1.16713	1.16
9	$3s\ ^2S\,3p^3(^2_3D)\ ^3D^\circ_3$	1.33333	1.33399	1.329
10	$3s\ ^2S\,3p^3(^2_3P)\ ^3P^\circ_2$	1.50000	1.48750	1.486
11	$3s\ ^2S\,3p^3(^2_1P)\ ^3P^\circ_1$	1.50000	1.50077	1.5
13	$3s^2\,3p\ ^2P\,3d\ ^1D^\circ_2$	1.00000	1.01330	1.014
15	$3s^2\,3p\ ^2P\,4s\ ^3P^\circ_1$	1.50000	1.49450	1.495
16	$3s^2\,3p\ ^2P\,4s\ ^3P^\circ_2$	1.50000	1.50106	1.499
17	$3s^2\,3p\ ^2P\,3d\ ^3F^\circ_2$	0.66667	0.66594	0.666
18	$3s^2\,3p\ ^2P\,3d\ ^3F^\circ_3$	1.08333	1.08347	1.083
19	$3s^2\,3p\ ^2P\,3d\ ^3F^\circ_4$	1.25000	1.25051	1.25
20	$3s^2\,3p\ ^2P\,4s\ ^1P^\circ_1$	1.00000	1.00644	1.006
21	$3s^2\,3p\ ^2P\,4p\ ^1P_1$	1.00000	0.99420	0.998
22	$3s^2\,3p\ ^2P\,4p\ ^3D_1$	0.50000	0.50942	0.511
23	$3s^2\,3p\ ^2P\,3d\ ^1P^\circ_1$	1.00000	0.99699	1
24	$3s^2\,3p\ ^2P\,4p\ ^3D_2$	1.16667	1.16808	1.166
25	$3s^2\,3p\ ^2P\,4p\ ^3D_3$	1.33333	1.33404	1.334
26	$3s^2\,3p\ ^2P\,3d\ ^3P^\circ_2$	1.50000	1.37568	1.408
27	$3s^2\,3p\ ^2P\,3d\ ^3D^\circ_1$	0.50000	0.89293	0.94
28	$3s^2\,3p\ ^2P\,3d\ ^3D^\circ_3$	1.33333	1.33335	1.326
29	$3s^2\,3p\ ^2P\,3d\ ^3P^\circ_1$	1.50000	1.11039	1.05
31	$3s^2\,3p\ ^2P\,3d\ ^3D^\circ_2$	1.16667	1.29222	1.26
33	$3s^2\,3p\ ^2P\,4p\ ^3P_1$	1.50000	1.53101	1.525
34	$3s^2\,3p\ ^2P\,4p\ ^3P_2$	1.50000	1.49802	1.499
35	$3s^2\,3p\ ^2P\,4p\ ^3S_1$	2.00000	1.96742	1.968
36	$3s^2\,3p\ ^2P\,3d\ ^1F^\circ_3$	1.00000	1.00063	1.004
37	$3s^2\,3p\ ^2P\,4p\ ^1D_2$	1.00000	1.00189	1.002
40	$3s\ ^2S\,3p^3(^2_3D)\ ^1D^\circ_2$	1.00000	1.00010	0.998
41	$3s\ ^2S\,3p^3(^2_1P)\ ^1P^\circ_1$	1.00000	1.00064	0.99
43	$3s^2\,3p\ ^2P\,5s\ ^3P^\circ_1$	1.50000	1.46648	1.465
44	$3s^2\,3p\ ^2P\,5s\ ^3P^\circ_2$	1.50000	1.50104	1.497
45	$3s^2\,3p\ ^2P\,5s\ ^1P^\circ_1$	1.00000	1.03443	1.036
46	$3s^2\,3p\ ^2P\,4d\ ^3F^\circ_2$	0.66667	0.66790	0.664
47	$3s^2\,3p\ ^2P\,4d\ ^3F^\circ_3$	1.08333	1.08425	1.081
48	$3s^2\,3p\ ^2P\,4d\ ^3F^\circ_4$	1.25000	1.25053	1.25
49	$3s^2\,3p\ ^2P\,4d\ ^3P^\circ_2$	1.50000	1.33882	1.278
50	$3s^2\,3p\ ^2P\,4d\ ^3D^\circ_1$	0.50000	0.89316	0.87
51	$3s^2\,3p\ ^2P\,4d\ ^1D^\circ_2$	1.00000	1.05416	1.098
52	$3s^2\,3p\ ^2P\,4d\ ^3D^\circ_3$	1.33333	1.33185	1.33
54	$3s^2\,3p\ ^2P\,4d\ ^3P^\circ_1$	1.50000	1.10772	1.129
55	$3s^2\,3p\ ^2P\,4d\ ^3D^\circ_2$	1.16667	1.27311	1.284
56	$3s^2\,3p\ ^2P\,5p\ ^1P_1$	1.00000	0.94599	0.94
57	$3s^2\,3p\ ^2P\,5p\ ^3D_1$	0.50000	0.63857	0.62
58	$3s^2\,3p\ ^2P\,5p\ ^3D_2$	1.16667	1.18244	1.187
59	$3s^2\,3p\ ^2P\,5p\ ^3D_3$	1.33333	1.33383	1.34
61	$3s^2\,3p\ ^2P\,5p\ ^3P_1$	1.50000	1.46729	1.473
62	$3s^2\,3p\ ^2P\,4d\ ^1F^\circ_3$	1.00000	1.00138	1
63	$3s^2\,3p\ ^2P\,5p\ ^3P_2$	1.50000	1.47622	1.47
64	$3s^2\,3p\ ^2P\,5p\ ^3S_1$	2.00000	1.95020	1.96
65	$3s^2\,3p\ ^2P\,4f\ ^1F_3$	1.00000	1.02861	1.02
66	$3s^2\,3p\ ^2P\,4f\ ^3F_2$	0.66667	0.69005	0.674
67	$3s^2\,3p\ ^2P\,4f\ ^3F_3$	1.08333	1.02328	1.03
68	$3s^2\,3p\ ^2P\,4f\ ^3F_4$	1.25000	1.21827	1.22
69	$3s^2\,3p\ ^2P\,5p\ ^1D_2$	1.00000	1.00737	1.005
70	$3s^2\,3p\ ^2P\,4f\ ^3G_3$	0.75000	0.79709	0.79
71	$3s^2\,3p\ ^2P\,4f\ ^3G_4$	1.05000	1.07055	1.06
72	$3s^2\,3p\ ^2P\,4f\ ^3G_5$	1.20000	1.20042	1.2
73	$3s^2\,3p\ ^2P\,4d\ ^1P^\circ_1$	1.00000	0.99914	0.999
74	$3s^2\,3p\ ^2P\,4f\ ^1G_4$	1.00000	1.01177	1.01
75	$3s^2\,3p\ ^2P\,4f\ ^3D_3$	1.33333	1.31820	1.32
76	$3s^2\,3p\ ^2P\,4f\ ^3D_2$	1.16667	1.06628	1.063
77	$3s^2\,3p\ ^2P\,4f\ ^3D_1$	0.50000	0.49893	0.5
78	$3s^2\,3p\ ^2P\,4f\ ^1D_2$	1.00000	1.07863	1.083
81	$3s^2\,3p\ ^2P\,6s\ ^3P^\circ_1$	1.50000	1.41849	1.42
85	$3s^2\,3p\ ^2P\,6s\ ^3P^\circ_2$	1.50000	1.50082	1.5
87	$3s^2\,3p\ ^2P\,6s\ ^1P^\circ_1$	1.00000	1.08220	1.08
89	$3s^2\,3p\ ^2P\,5d\ ^3F^\circ_2$	0.66667	0.68597	0.69
90	$3s^2\,3p\ ^2P\,5d\ ^3F^\circ_3$	1.08333	1.09022	1.08
91	$3s^2\,3p\ ^2P\,5d\ ^3F^\circ_4$	1.25000	1.25053	1.25
93	$3s^2\,3p\ ^2P\,5d\ ^1D^\circ_2$	1.00000	1.13551	1.12
94	$3s^2\,3p\ ^2P\,5d\ ^3D^\circ_1$	0.50000	0.70581	0.69
95	$3s^2\,3p\ ^2P\,5d\ ^3D^\circ_2$	1.16667	1.17731	1.18
96	$3s^2\,3p\ ^2P\,5d\ ^3D^\circ_3$	1.33333	1.32274	1.33
97	$3s^2\,3p\ ^2P\,5d\ ^3P^\circ_2$	1.50000	1.33546	1.34
98	$3s^2\,3p\ ^2P\,5d\ ^3P^\circ_1$	1.50000	1.29786	1.3
101	$3s^2\,3p\ ^2P\,5d\ ^1F^\circ_3$	1.00000	1.00454	1.01
	Si I [1]			
2	$3p^2(^3_2P)\ ^3P_1$	1.50000	1.50110	1.52
3	$3p^2(^3_2P)\ ^3P_2$	1.50000	1.50095	1.50
4	$3p^2(^1_2D)\ ^1D_2$	1.00000	1.00009	1.01
8	$3p\ ^2P\,4s\ ^3P^\circ_1$	1.50000	1.49593	1.52
9	$3p\ ^2P\,4s\ ^3P^\circ_2$	1.50000	1.50110	1.49
10	$3p\ ^2P\,4s\ ^1P^\circ_1$	1.00000	1.00509	0.99
15	$3p\ ^2P\,3d\ ^1D^\circ_2$	1.00000	1.00005	1.02
32	$3p\ ^2P\,3d\ ^1P^\circ_1$	1.00000	0.99476	1.00
	Si III [1]			
5	$3s\,3p\ ^1P^\circ_1$	1.00000	0.99995	0.98
6	$3p^2\ ^1D_2$	1.00000	1.00010	0.98
13	$3s\,4s\ ^3S_1$	2.00000	2.00221	2.00
16	$3s\,3d\ ^1D_2$	1.00000	0.99996	0.99
18	$3s\,4p\ ^3P^\circ_1$	1.50000	1.50050	1.55
19	$3s\,4p\ ^3P^\circ_2$	1.50000	1.50109	1.49
20	$3s\,4p\ ^1P^\circ_1$	1.00000	1.00054	1.01
27	$3s\,4d\ ^1D_2$	1.00000	1.00000	1.00
	Si IV [1]			
6	$4s\ ^2S_{1/2}$	2.00000	2.00225	1.98
7	$4p\ ^2P^\circ_{1/2}$	0.670000	0.66583	0.72
8	$4p\ ^2P^\circ_{3/2}$	1.33000	1.33405	1.34
9	$4d\ ^2D_{5/2}$	1.20000	1.20043	1.16
15	$5p\ ^2P^\circ_{3/2}$	1.33000	1.33407	1.34
	Ti II [4]			
11	$3d^2(^1_2D)\ ^1D\,4s\ ^2D_{3/2}$	0.800000	0.80900	0.80
15	$3d^3(^4_3P)\ ^4P_{1/2}$	2.66667	2.58681	2.63
16	$3d^3(^4_3P)\ ^4P_{3/2}$	1.73333	1.70373	1.74
18	$3d^3(^2_3P)\ ^2P_{1/2}$	0.666667	0.78123	0.66
19	$3d^2(^3_2P)\ ^3P\,4s\ ^4P_{1/2}$	2.66667	2.63809	2.60
21	$3d^3(^2_3P)\ ^2P_{3/2}$	1.33333	1.35842	1.33
29	$3d^2(^3_2P)\ ^3P\,4s\ ^2P_{1/2}$	0.666667	0.66607	0.66
30	$3d^2(^3_2P)\ ^3P\,4s\ ^2P_{3/2}$	1.33333	1.33324	1.33
45	$3d^2(^3_2F)\ ^3F\,4p\ ^2D^\circ_{3/2}$	0.800000	0.80021	0.92
46	$3d^2(^3_2F)\ ^3F\,4p\ ^2D^\circ_{5/2}$	1.20000	1.19159	1.20
48	$3d^2(^3_2F)\ ^3F\,4p\ ^4D^\circ_{1/2}$	0.000000	1.02735E-04	0.00
49	$3d^2(^3_2F)\ ^3F\,4p\ ^4D^\circ_{3/2}$	1.20000	1.18881	1.20
50	$3d^2(^3_2F)\ ^3F\,4p\ ^4D^\circ_{5/2}$	1.37143	1.36075	1.37
56	$3d^2(^3_2P)\ ^3P\,4p\ ^2S^\circ_{1/2}$	2.00000	1.99657	2.09
57	$3d^2(^1_2D)\ ^1D\,4p\ ^2D^\circ_{3/2}$	0.800000	0.98131	1.21
	Sn II [5]			
3	$5s\,5p^2\ ^4P_{1/2}$	2.66667	2.65984	2.6609

References. (1) Lott et al. (1966); (2) Li (1972); (3) Martin et al. (1985); (4) Moore (1949); (5) David et al. (1980).

Table A.2. Summary of levels with a relative difference ≥10% with respect to $g_J(LS)$.

No.	State	$g_J(LS)$	$g_{\gamma J}$	Kurucz
		C I		
60	$2p\ ^2P\ 4d\ ^3D^\circ_1$	0.50000	0.55335	0.527
69	$2p\ ^2P\ 4f\ ^3G_3$	0.75000	0.83619	0.808
82	$2p\ ^2P\ 5p\ ^3D_1$	0.50000	0.55210	0.610
92	$2p\ ^2P\ 5d\ ^3F^\circ_2$	0.66667	0.75711	0.733
96	$2p\ ^2P\ 5d\ ^3D^\circ_1$	0.50000	0.59981	0.604
97	$2p\ ^2P\ 6s\ ^3P^\circ_2$	1.50000	1.31673	1.342
99	$2p\ ^2P\ 5d\ ^3D^\circ_2$	1.16667	1.28419	1.277
		Si I		
40	$3p\ ^2P\ 4d\ ^1D^\circ_{2a}$	1.00000	1.23605	1.093
41	$3p\ ^2P\ 4d\ ^1D^\circ_{2b}$	1.00000	1.26057	1.403
45	$3p\ ^2P\ 5p\ ^3D_1$	0.50000	0.66751	0.698
58	$3p\ ^2P\ 4f\ ^3F_2$	0.66667	0.76027	0.755
59	$3p\ ^2P\ 4f\ ^3G_{3a}$	0.75000	0.89982	0.910
63	$3p\ ^2P\ 4f\ ^3G_{3b}$	0.75000	0.88920	0.881
68	$3p\ ^2P\ 4d\ ^3D^\circ_1$	0.50000	0.62064	0.554
81	$3p\ ^2P\ 6p\ ^3D_{1a}$	0.50000	0.75851	0.696
83	$3p\ ^2P\ 6p\ ^3D_{1b}$	0.50000	1.10995	1.363
96	$3p\ ^2P\ 5f\ ^3F_{2a}$	0.66667	0.81795	0.814
97	$3p\ ^2P\ 5f\ ^3G_3$	0.75000	0.92167	0.873
99	$3p\ ^2P\ 5g\ ^3G^\circ_{3a}$	0.75000	0.89339	0.894
111	$3p\ ^2P\ 5f\ ^3F_{2b}$	0.66667	0.91694	0.923
116	$3p\ ^2P\ 5g\ ^3G^\circ_{3b}$	0.75000	0.89222	0.891
131	$3p\ ^2P\ 7p\ ^3D_1$	0.50000	0.69044	0.672
134	$3p\ ^2P\ 6d\ ^3F^\circ_{2a}$	0.66667	0.88297	0.866
137	$3p\ ^2P\ 6d\ ^3F^\circ_{2b}$	0.66667	0.82644	0.855
138	$3p\ ^2P\ 7p\ ^1P_1$	1.00000	1.14422	1.299
144	$3p\ ^2P\ 6f\ ^3G_3$	0.75000	0.83711	1.147
147	$3p\ ^2P\ 6f\ ^3F_{2a}$	0.66667	0.85004	0.850
152	$3p\ ^2P\ 6d\ ^1F^\circ_3$	1.00000	1.10913	1.031
157	$3p\ ^2P\ 6f\ ^3F_{2b}$	0.66667	0.88535	0.892
		P II		
27	$3s^2\ 3p\ ^2P\ 3d\ ^3D^\circ_1$	0.50000	0.89293	0.940
29	$3s^2\ 3p\ ^2P\ 3d\ ^3P^\circ_1$	1.50000	1.11039	1.050
31	$3s^2\ 3p\ ^2P\ 3d\ ^3D^\circ_2$	1.16667	1.29222	1.260
49	$3s^2\ 3p\ ^2P\ 4d\ ^3P^\circ_2$	1.50000	1.33882	1.278
50	$3s^2\ 3p\ ^2P\ 4d\ ^3D^\circ_1$	0.50000	0.89316	0.870
54	$3s^2\ 3p\ ^2P\ 4d\ ^3P^\circ_1$	1.50000	1.10772	1.129
57	$3s^2\ 3p\ ^2P\ 5p\ ^3D_1$	0.50000	0.63857	0.620
93	$3s^2\ 3p\ ^2P\ 5d\ ^1D^\circ_2$	1.00000	1.13551	1.120
94	$3s^2\ 3p\ ^2P\ 5d\ ^3D^\circ_1$	0.50000	0.70581	0.690
97	$3s^2\ 3p\ ^2P\ 5d\ ^3P^\circ_2$	1.50000	1.33546	1.340
98	$3s^2\ 3p\ ^2P\ 5d\ ^3P^\circ_1$	1.50000	1.29786	1.300
		S II		
87	$3s^2\ 3p^2(^1_0S)\ ^1S\ 4p\ ^2P^\circ_{1/2}$	0.66667	0.84052	0.945
102	$3s\ ^2S\ 3p^4(^3_2P)\ ^2P_{3/2}$	1.33333	1.15616	
104	$3s^2\ 3p^2(^3_2P)\ ^3P\ 4f\ ^4D^\circ_{7/2}$	1.42857	1.23570	1.281
106	$3s^2\ 3p^2(^3_2P)\ ^3P\ 4d\ ^2D_{3/2}$	0.80000	0.97639	0.887
107	$3s^2\ 3p^2(^3_2P)\ ^3P\ 4f\ ^2D^\circ_{5/2}$	1.20000	0.94834	0.930
108	$3s^2\ 3p^2(^3_2P)\ ^3P\ 4f\ ^4G^\circ_{7/2}$	0.98413	1.14087	1.109
111	$3s^2\ 3p^2(^3_2P)\ ^3P\ 4f\ ^4D^\circ_{3/2}$	1.20000	0.92391	0.919
114	$3s^2\ 3p^2(^3_2P)\ ^3P\ 4f\ ^2D^\circ_{3/2}$	0.80000	0.99823	1.005
118	$3s^2\ 3p^2(^3_2P)\ ^3P\ 4f\ ^4F^\circ_{3/2}$	0.40000	0.47703	0.475
		Cl III		
18	$3s^2\ 3p^2(^3_2P)\ ^3P\ 3d\ ^4D_{5/2}$	1.37143	1.17635	1.359
22	$3s^2\ 3p^2(^1_2D)\ ^1D\ 3d\ ^2F_{5/2}$	0.85714	1.05128	0.873
		Ar IV		
18	$3s^2\ 3p^2(^1_2D)\ ^1D\ 3d\ ^2F_{5/2}$	0.85714	1.02081	0.861
22	$3s^2\ 3p^2(^3_2P)\ ^3P\ 3d\ ^4D_{5/2}$	1.37143	1.20618	1.184
101	$3s\ ^2S\ 3p^3(^2_1P)\ ^3P\ 3d\ ^2D^\circ_{5/2}$	1.20000	1.34088	1.202
		Ca I		
13	$3s^2\ 3p^6\ 3d\ ^2D\ 4p\ ^3F^\circ_2$	0.66667	0.74211	0.754
		Ti II		
18	$3d^3(^2_3P)\ ^2P_{1/2}$	0.66667	0.78123	0.660
57	$3d^2(^1_2D)\ ^1D\ 4p\ ^2D^\circ_{3/2}$	0.80000	0.98131	1.210
59	$3d^2(^1_2D)\ ^1D\ 4p\ ^2P^\circ_{3/2}$	1.33333	1.19437	1.200
81	$3d\ ^2D\ 4s\ ^3D\ 4p\ ^4F^\circ_{3/2}$	0.40000	0.54562	0.462
83	$3d\ ^2D\ 4s\ ^3D\ 4p\ ^4F^\circ_{5/2}$	1.02857	1.13809	1.078
84	$3d\ ^2D\ 4s\ ^3D\ 4p\ ^4D^\circ_{3/2}$	1.20000	1.05899	1.140
		Zr III		
16	$4d\ ^2D\ 5p\ ^3F^\circ_2$	0.66667	0.77976	0.807
34	$4d\ ^2D\ 5d\ ^3G_{3a}$	0.75000	1.01649	0.925
35	$4d\ ^2D\ 5d\ ^3G_{3b}$	0.75000	1.05195	1.146
36	$4d\ ^2D\ 6s\ ^3D_1$	0.50000	0.63883	0.630
39	$4d\ ^2D\ 5d\ ^1P_1$	1.00000	0.89734	0.887
48	$4d\ ^2D\ 5d\ ^1D_2$	1.00000	1.13456	1.110
50	$4d\ ^2D\ 5d\ ^3P_2$	1.50000	1.35112	1.373
55	$4d\ ^2D\ 6p\ ^3D^\circ_2$	1.16667	0.92822	1.034
76	$4d\ ^2D\ 4f\ ^3D^\circ_1$	0.50000	0.59790	0.605
77	$4d\ ^2D\ 4f\ ^3D^\circ_3$	1.33333	1.17260	1.175
79	$4d\ ^2D\ 4f\ ^1F^\circ_3$	1.00000	1.13107	1.126
		Sn II		
13	$5s\ 5p^2\ ^2S_{1/2}$	2.00000	1.36349	
14	$5s\ 5p^2\ ^2P_{1/2}$	0.66667	1.31877	

Notes. Kurucz's data (Kurucz 2017) are shown in the last column for comparision.